communications earth & environment

ARTICLE

https://doi.org/10.1038/s43247-021-00304-6 OPEN

Onset and termination of Heinrich Stadial 4 and the underlying climate dynamics

Hai Cheng[1,2,3✉], Yao Xu[1], Xiyu Dong[1], Jingyao Zhao[1], Hanying Li[1], Jonathan Baker[1], Ashish Sinha[4], Christoph Spötl[5], Haiwei Zhang[1], Wenjing Du[1], Baoyun Zong[1], Xue Jia[1], Gayatri Kathayat[1], Dianbing Liu[6], Yanjun Cai[1], Xianfeng Wang[7], Nicolás M. Strikis[8], Francisco W. Cruz[8], Augusto S. Auler[9], Anil K. Gupta[10], Raj Kumar Singh[11], Sonu Jaglan[12], Som Dutt[13], Zhengyu Liu[14] & R. Lawrence Edwards[15]

Heinrich Stadial 4 during the last glacial period was marked by severe cooling at northern high latitudes along with the attendant changes in Asian Monsoon (Chinese Stadial 4) and South American Monsoon (South American Stadial 4). Here we present improved constraints on timings of Heinrich/Chinese/South American Stadial 4 onset and termination at sub-centennial precision based on speleothem records. We show that their initial onsets were essentially synchronous (40.20 ± 0.08 thousand years ago) and led the Antarctic warming by ~300 years. The Heinrich/Chinese Stadial 4 termination commenced at 38.34 ± 0.07 thousand years ago following a centennial-scale reduction in the Amazon River runoff and a poleward shift of the Southern Westerly wind belt. These two precursor events may have contributed to a reduced Amazon Plume Region and an enhanced Agulhas salt/heat leakage that led to an abrupt resumption of the Atlantic Meridional Ocean Circulation eventually triggering the Heinrich/Chinese Stadial 4 termination.

[1] Institute of Global Environmental Change, Xi'an Jiaotong University, 710054 Xi'an, China. [2] State Key Laboratory of Loess and Quaternary Geology, Institute of Earth Environment, Chinese Academy of Sciences, 710061 Xi'an, China. [3] Key Laboratory of Karst Dynamics, MLR, Institute of Karst Geology, CAGS, 541004 Guilin, China. [4] Department of Earth Sciences, California State University Dominguez Hills, CA 90747 Carson, USA. [5] Institute of Geology, University of Innsbruck, 6020 Innsbruck, Austria. [6] College of Geography Science, Nanjing Normal University, Nanjing, China. [7] Earth Observatory of Singapore, Nanyang Technological University, Singapore 639798, Singapore. [8] Instituto de Geociências, Universidade de São Paulo, São Paulo 05508-090, Brazil. [9] Instituto do Carste, Rua Barcelona 240/302, Belo Horizonte, Minas Gerais 30360-260, Brazil. [10] Department of Geology and Geophysics, Indian Institute of Technology Kharagpur, Kharagpur, India. [11] School of Earth, Ocean and Climate Sciences, Indian Institute of Technology Bhubaneswar, Argul 752050, India. [12] Department of Geology, Govt. P. G. College Narnaul, Mahendragarh 123001, India. [13] Wadia Institute of Himalayan Geology, Dehradun 248001, India. [14] Department of Geography, The Ohio State University, Columbus, OH, USA. [15] Department of Earth and Environmental Sciences, University of Minnesota, MN 55455 Minneapolis, USA. ✉email: cheng021@xjtu.edu.cn

The last glacial period was characterized by a series of global-scale abrupt millennial-climate events known as Dansgaard–Oeschger (DO) cold stadials and warm interstadials[1]. Heinrich events contain layers of ice-rafted debris indicative of massive iceberg discharges into the North Atlantic[2–4]. The cold stadials containing the Heinrich events are also referred to as Heinrich Stadial (HS)[5,6]. HSs were marked by widespread cooler and drier conditions across large regions of North America, Eurasia, and North Africa[7–10]. A southward displacement of the Intertropical Convergence Zone (ITCZ) and a weakening of Northern Hemisphere (NH) Asian summer monsoon (namely Chinese Stadials (CSs))[11] was associated, whereas many regions in the Southern Hemisphere (SH), especially the Amazon Basin, became wetter due to associated intensification of the summer monsoons (hereafter, South American Stadials (SASs)), which are nearly anti-correlated to CSs[12–18]. Meanwhile, Antarctica experienced warmer temperatures consistent with a reduction of the northward heat transport from SH to NH via for example, the Atlantic Meridional Ocean Circulation (AMOC)[19]. These scenarios manifest an important aspect of the global thermal seesaw[20–23].

In the past three decades, six HSs and corresponding hydroclimate anomalies CSs/SASs (1–6) have been recognized during the last glacial period with a ~7 ky (thousand years) quasi-periodic recurrence[2,11]. Among them, HS4 contains the ice-rafted debris originated from the Laurentide Ice Sheet, similar to HS0 (the Younger Dryas)[24,25]. A large number of observational and modeling studies attribute HSs to the weakening of the AMOC in response to the release of freshwater by melting icebergs[26–28]. Consistently, recent studies have shown that the abrupt onset of Greenland warming (cooling) led the corresponding Antarctic cooling (warming) onset by ~200 ± 100 y, implying a north–south propagation of abrupt climatic signals[29]. Subsequent ice-core studies have also found that the meridional migration of the SH Westerly Wind (SWW) belt and the ITCZ, two key components of the global atmospheric circulation implicated in the DO-related climate changes, were in phase with Greenland HSs, suggesting a fast NH to SH directionality of global atmospheric teleconnection[21,23,30,31]. On the other hand, on the basis of precisely dated speleothem $\delta^{18}O$ records, combined with polar ice-core records, the evolution of SH or tropical Pacific temperature/hydroclimate likely played an active role in DO variability/Greenland climate dynamics[23], as hypothesized previously in a number of studies but were based mostly on numerical models or low-resolution data with loosely constrained chronologies[32–36]. These developments, therefore, warrant further investigation of the phase relationship of millennial-scale events between different climate systems during the glacial period and their underlying mechanisms[23,37].

Here, we report a set of new-generation speleothem $\delta^{18}O$ records of CS4/SAS4 from Asian Monsoon (AM) and South American Monsoon (SAM) domains. We compare these data with a suite of previously published speleothem and ice-core records, and provide a synthesis of HS4 and associated CS4/SAS4 across different regimes. By focusing on the relative timing and structure of HS4, CS4, and SAS4 in each region, we aim to identify the dynamics associated with their onset and termination. Our results shed light on the underlying dynamics of the stadials, particularly with respect to their terminations.

Speleothem samples

In this study, we have developed and, in some cases, considerably improved the chronological frameworks of ten speleothem $\delta^{18}O$ records from the AM and SAM domains. The AM cave records include Hulu (MSL, 32°30′N, 119°10′E)[38], Mawmluh (MWS-2, 25°16′N, 91°43′E)[39], Zhangjia (ZJD171, 32°35′N, 105°58′E), and Wulu (Wulu-30, 26°03′N, 105°05′E)[40]. The EL Condor (ELC-B, 5°56′S, 77°18′W)[12], Paraiso (PAR27 and PAR15, 4°04′S, 55°27′W)[14], Lapa Sem Fim (LSF13, 16°09′S, 44°36′W)[41] and Toca da Boa Vista/Toca da Barriguda (TBV5 and TBR10-13, 10°10′S, 40°52′W)[42,43] records are from the SAM domain (including the Amazon Basin). Cave locations are shown in Supplementary Fig. 1. Climatic significances of these records are outlined in the aforementioned references. In short, the speleothem $\delta^{18}O$ records from these two monsoon domains have been interpreted to reflect the overall intensity of monsoon rainfall/circulation and/or north-south shifts of the ITCZ[12,14,18,23,42,44–46].

The speleothem chronologies are based on extensive U-Th dating (~130 dates) by an improved technique[47]. The dating work was performed at the Isotope Laboratory of Xi'an Jiaotong University, using Multi-collector Inductively Coupled Plasma Mass Spectrometry (MC-ICP-MS, see "Methods" section). Typical age uncertainties (2σ) vary between 60 and 150 y for most key intervals (Supplementary Data 1). The age models of speleothem $\delta^{18}O$ records were constructed using StalAge[48] (Supplementary Fig. 2). This algorithim estimates the uncertainty window of interpolated ages iteratively by using a Monte Carlo simulation ($N = 300$) (see "Methods" section). A total of ~3550 oxygen-isotope ($\delta^{18}O$) subsamples were analyzed at the Instituto de Geociências, Universidade de São Paulo, Brazil (sample LSF13) and Xi'an Jiaotong University, China (the remaining nine samples) (Supplementary Data 1). The $\delta^{18}O$ values are reported in permil (‰) deviations, relative to the Vienna Pee Dee Belemnite standard. The long-term reproducibility for $\delta^{18}O$ measurements at both laboratories is typically ~0.1‰ (1σ) (see "Methods" section).

Results and discussion

Speleothem $\delta^{18}O$ records. Recently, we used a correlation strategy that relies on using "breakpoints" instead of conventional "mid-points" for correlating the HS0 among the AM-AW (Asian Westerlies) and Greenland ice-core $\delta^{18}O$ records[23] in the NH (Supplementary Fig. 3a). In this study, we have adopted a similar strategy to determine the initial onset and termination of HS4/CS4/SAS4 from precisely dated high-resolution speleothem $\delta^{18}O$ records. This strategy employs identification of the breakpoints and their temporal uncertainties from the visual inspection of $\delta^{18}O$ profiles (Method 1, see "Methods" section) together with more objective determinations of breakpoints by using the BREAKFIT algorithm[49]. Using this approach, we conducted BREAKFIT analysis using both individual records as well as their regional composites. To account for the dating uncertainties and time-series "noise" (i.e., differences in $\delta^{18}O$ profiles from the same region), we repeated the analysis using the 2.5th, 50th, and 97.5th percentile of StalAge-derived age model ensembles for each record and their composite (Methods 2 and 3, see "Methods" section).

Based on the visual inspections alone, we identified the initial onset of CS4 in AM-AW records (i.e., the approximate $\delta^{18}O$ minima) at 40.24 ± 0.12 ky BP (MWS-2), 40.21 ± 0.09 ky BP (ZJD171), 40.20 ± 0.06 ky BP (Wulu-30), and 40.14 ± 0.10 ky BP (So-1). The So-1 record is from Sofular cave in the AW region[50] (Figs. 1 and 2). The error-weighted average age of CS4 initial onset from these records is 40.20 ± 0.05 (2σ) ky BP. The initial onset of SAS4 in the SAM records (i.e., the approximate $\delta^{18}O$ maxima) is 40.20 ± 0.10 ky BP (PAR15), 40.22 ± 0.07 ky BP (PAR27), and 40.15 ± 0.06 ky BP (LSF13) with an error-weighted mean of 40.19 ± 0.05 (2σ) ky BP (Fig. 1 and Supplementary Figs. 2–4 and Supplementary Tables 1–3 and Supplementary Data 1). For both CS4 and SAS4 records, the error-weighted

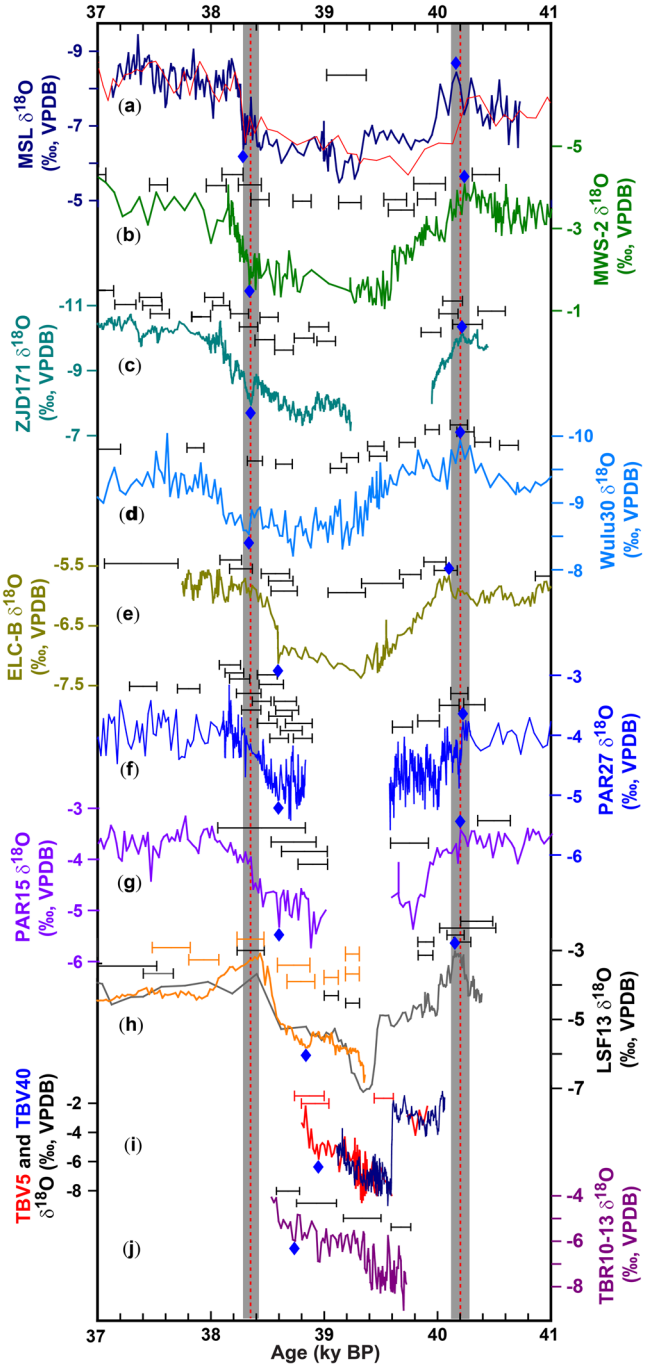

Fig. 1 Speleothem $\delta^{18}O$ records from AM and SAM monsoon domains. **a**–**e** Speleothem $\delta^{18}O$ records from Hulu (MSL) (dark blue—this study; red—from the previous study[38]), Mawmluh (MWS-2)[39], Zhangjia (ZJD171) (this study) and Wulu (Wulu-30, this study)[40] caves in the AM domain. **e**–**j** Speleothem $\delta^{18}O$ records from El-Condor (ELC-B)[12], Paraiso (PAR27 and PAR15, this study)[14], Lapa Sem Fim (LSF13, gray and orange curves: low and high-resolution data, this study)[41], Toca da Boa Vista (TBV5 (red): this study; TBV40 (dark blue)[42]), and Toca da Barriguda (TBR10-13: this study)[42,43] caves in the SAM domain. Cave locations are shown in Supplementary Fig. 1. Error bars show U-Th dates (2σ) for each record. The Hulu (MSL) chronology is based on the previous study[38] and the error bar depicts the typical uncertainty. Two vertical dashed lines depict the initial onset of CS4/SAS4 at 40.20 ± 0.08 ky BP and initial CS4 termination at 38.34 ± 0.07 ky BP, respectively. Vertical dark gray bars show the uncertainties. Blue diamonds show the initial onset and termination points determined directly based on the Method 1.

average of their breakpoint ages is 40.20 ± 0.04 ky BP with a 2σ uncertainty of ±0.07 ky BP. We surmise that the error-weighted uncertainty and standard deviation reflect the age model uncertainty and the proxy time-series noise, therefore, by quadratically combining these errors, we derive the breakpoint age of 40.20 ± 0.08 ky BP as the anchor point of the initial onset of CS4/SAS4 for correlating hydroclimate records, especially those that have large absolute but small relative chronology uncertainties, such as ice-core records. This estimate is consistent with the timing and uncertainty of the corresponding "breakpoints" determined via Method 2 and Method 3 (Fig. 1 and Supplementary Figs. 4 and 5, Supplementary Tables 1–3 and Supplementary Data 1, see "Methods" section).

In contrast to their synchronous onset, the timings of the initial termination of the monsoon anomalies between CS4 and SAS4 are apparently different. The timings (i.e., the $\delta^{18}O$ maxima around the initial termination) are 38.33 ± 0.07 ky BP (MWS-2), 38.35 ± 0.06 (ZJD171), and 38.33 ± 0.06 (Wulu-30) with an error weighted average of 38.34 ± 0.04 ky BP from the AM regime, consistent within errors with the So-1 record (~38.40 ± 0.10 ky BP) from the AW regime (Figs. 1 and 2 and Supplementary Fig. 4 and Supplementary Tables 1–3 and Supplementary Data 1). The error from Method 3 (±0.07 ky, Supplementary Fig. 4) is larger than the quadratically combined 2σ uncertainty and error-weighted mean uncertainty (±0.05 ky), and therefore, we used the timing of ~38.34 ± 0.07 ky BP as another important anchor point. The identification of breakpoints from BREAKFIT algorithm (Method 2 and Method 3) are consistent within uncertainty with this result (Fig. 1; Supplementary Figs. 4 and 5 and Supplementary Tables 1–3 and Supplementary Data 1, see "Methods" section). Notably, the timing of the SAS4 initial termination appears to be earlier: ~38.70 ± 0.07 ky BP (PAR27), ~38.59 ± 0.23 ky BP (PAR15), and ~38.60 ± 0.07 ky BP (ELC-B) in Amazonia (Supplementary Figs. 4–6 and Supplementary Tables 1–3 and Supplementary Data 1), although the large uncertainties preclude a definitive conclusion. Yet, more robust supportive evidence comes from the records in eastern Brazil. The LSF13 record shows a rather earlier SAS4 initial termination at ~38.85 ± 0.11 in central-eastern Brazil. The records from Toca da Boa Vista/Toca da Barriguda caves, northeastern Brazil show the drying trend inferred by $\delta^{18}O$ records started even much earlier (at ~39.5 ky BP) and ended by a growth hiatus at ~38.6 ky BP, implying an arid condition similar to pre-SAS4 and post-SAS4 (Figs. 1 and 3 and Supplementary Fig. 6). As such, the observed initial termination of SAS4 appears to lead the anchor point (38.34 ± 0.07 ky BP) by a few to several hundred years (Fig. 3 and Supplementary Figs. 4–6).

Correlation of Greenland ice-core records to Asian monsoon records. The current chronologies of Greenland ice-core records largely rely on the annual band counting of the North Greenland Ice-core Project (NGRIP) ice-core (i.e., the GICC05 chronology). The absolute age uncertainty of GICC05 remains significant, ca. ±1500 (2σ) y at the HS4 interval[51,52], which theoretically precludes correlations with other climate records at sub-centennial/centennial precision. Although speleothem records provide much more precise age constraints on HS4, the transfer of speleothem chronologies to ice-core relies on a proper correlation strategy. Recent studies of HS0 and Greenland Stadial (GS) 20 (or "HS7") have established a synchronization strategy that utilizes breakpoints rather than mid-points, assuming a causal synchroneity between abrupt Greenland temperature change and the initial AM-AW response[23,53]. Crucially, the breakpoint strategy was validated via dating of speleothem HS0 records from the North

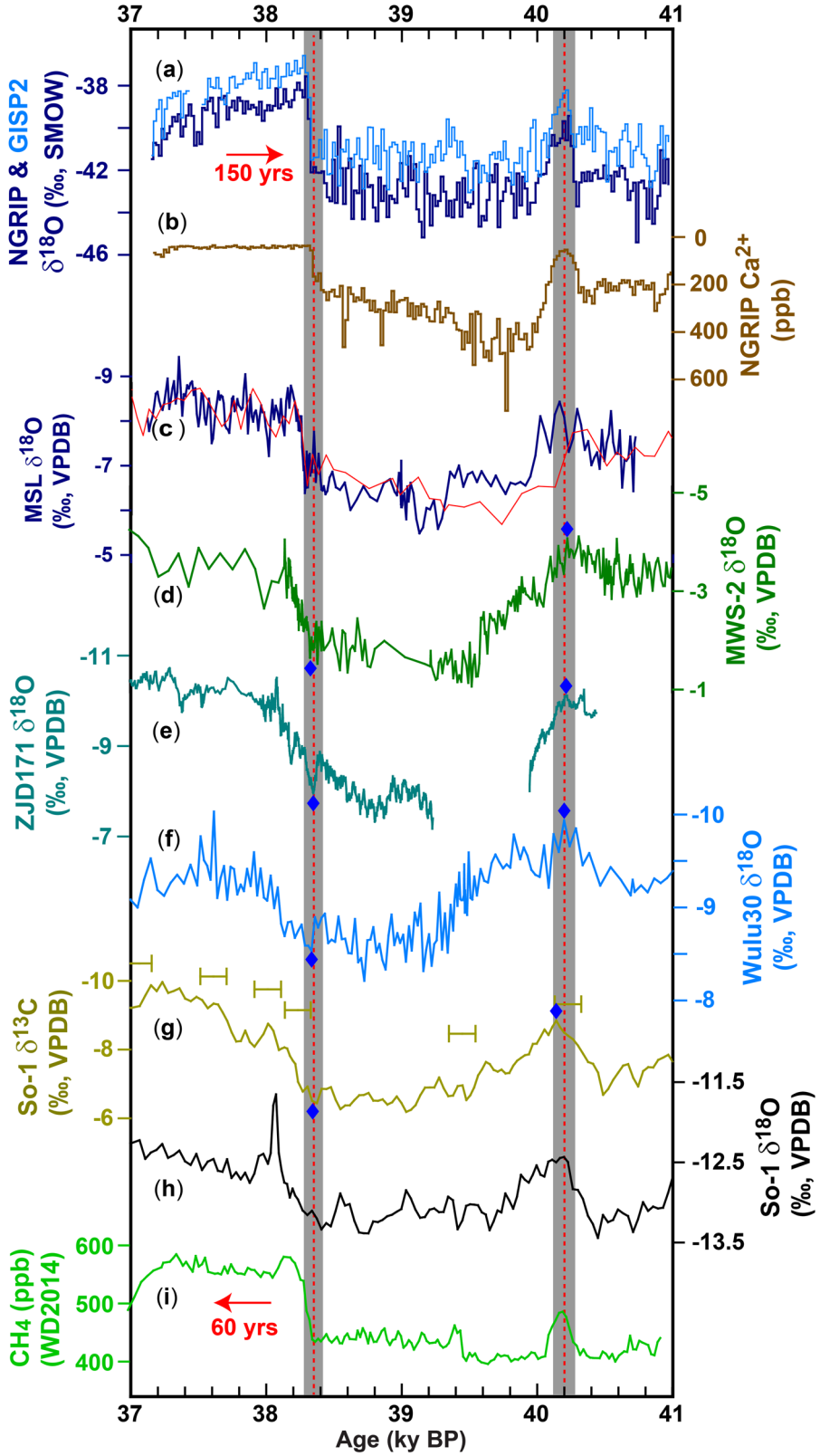

Fig. 2 Correlation between Greenland ice-core and AM speleothem records. a, **b** Greenland NGRIP $\delta^{18}O$ and Ca^{2+} records on the GICC05 chronology[1] with a +150 y shift (red arrow) based on the "breakpoint" correlation with AM records[23] (also see text and Supplementary Fig. 3). **c**–**f** Speleothem $\delta^{18}O$ records from Hulu, Mawmluh, Zhangjia, and Wulu caves in the AM domain (Fig. 1). **g**, **h** So-1 $\delta^{13}C$ and $\delta^{18}O$ records from Sofular cave in Turkey, indicating the AW ecosystem and climate changes[50]. **i** CH_4 record from the Antarctic WDC ice-core on the WD2014 chronology[60]. The WD2014 chronology is shifted by −60 years (red arrow) based on the breakpoint correlation of CH_4 with AM records[23]. Error bars in **g** show the U-Th dates (2σ). The vertical dashed lines, bars and blue diamonds are as same as in Fig. 1.

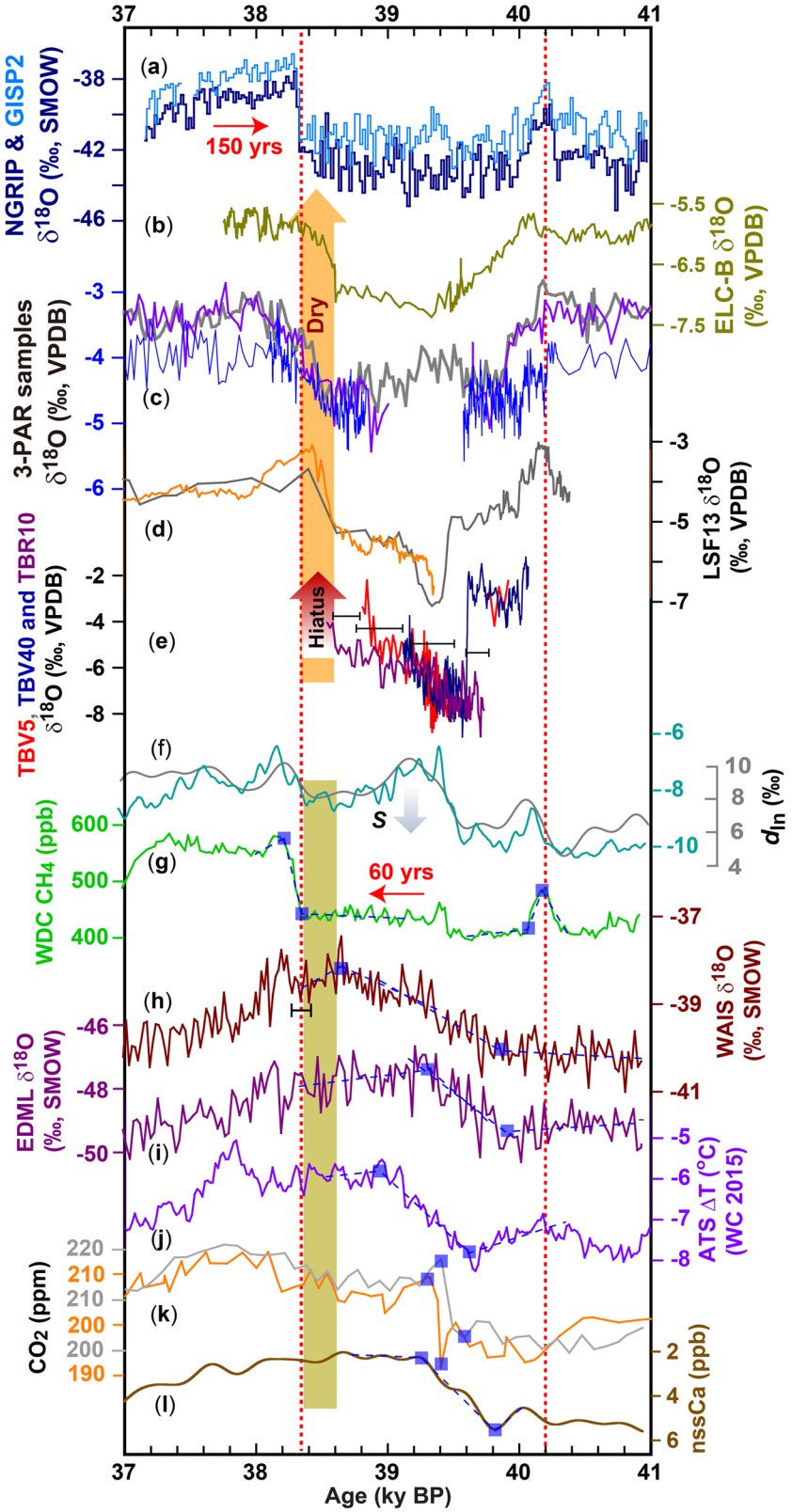

Atlantic and AM-AW domains showing synchroneity within a few decades[23].

On the basis of the HS0 synchroneity tested on decadal-scale between Greenland ice-core and AM-AW speleothem $\delta^{18}O$ records[23] in the NH, we correlate the initial $\delta^{18}O$ decrease in the NGRIP record around the HS4 onset to the 40.20 ± 0.08 ky BP anchor point from AM-AW and SAM records, and the initial $\delta^{18}O$ jump at the HS4 termination in the NGRIP record to the anchor point at 38.34 ± 0.07 ky BP from AM-AW records by shifting the GICC05 chronology to the older side by 150 y, well within its quoted absolute age uncertainty of ~1500 y (Fig. 2). This shift does not require a change of the relative age of the ice-core chronology, which is consistent with the fact that the ice-core record has a much smaller uncertainty in its relative age

Fig. 3 Comparison between polar ice-core and SAM speleothem records. a Same as **a** in Fig. 2. **b**–**e** Speleothem $\delta^{18}O$ records from the SAM domain. **b** Speleothem records from EL Condor Cave (ELC-B, this study). **c** Speleothem records from Paraiso Cave. Blue and purple curves: PAR27 and PAR15 records (this study). Gray curve: PAR07 record[14]. **d** Record from Lapa Sem Fim Cave (LSF13, gray and orange curves: low and high-resolution data, this study). **e** Speleothem records from Toca da Boa Vista (TBV)/Toca da Barriguda (TBR) caves (red and dark blue: TBV5 (this study) and TBV40[42]; purple: TBR10-13, this study). The red vertical arrow marks the speleothem growth hiatus. Error bars show the U-Th dates (2σ) of TBR10-13. **f** Antarctic deuterium-excess records (d_{ln}, a proxy for vapor source condition) on the WD2014 chronology[60]. Jade curve: 5-core average d_{ln} anomaly[21], gray curve: WDC d_{ln} record[30]. **g**, **h** CH_4 and $\delta^{18}O$ records from the Antarctic WDC ice-core on WD2014 chronology[60]. WD2014 chronology was shifted by −60 years based on the breakpoint correlation of CH_4 with AM records[23]. The black error bar depicts the uncertainty (~ ±75 years) of the WDC gas-ice age difference[60]. **i** The $\delta^{18}O$ record from the Antarctic EDML ice-core on WD2014 chronology)[60] with −60 year shift. **j** Antarctic temperature stack (ATS) record relative to the present day (ΔT) on the WC2015 chronology[63]. **k** Atmospheric CO_2 records (gray; orange on WD2014 chronology)[60,91]. **l** WDC non sea-salt Ca^{2+} ($nssCa^{2+}$) record (WD2014 chronology)[92]. High-frequency variability (>1/300 y^{-1}) removed with a low-pass Butterworth filter. Two vertical dashed lines are the same as in Fig. 2. Dashed blue lines and squares depict trends and breakpoints. The vertical gray arrow in **f** depicts the direction of poleward shift inferred by the d_{ln} change. The vertical orange arrow indicates the main termination (drying) trend ~250 y before 38.34 ky BP in SAM records, and the olive bar highlights changes/states of the other records during the same period.

(< 200 y across HS4)[54]. An apparent age difference of ~250 ± 500 (2σ) y around HS4 between cave and ice-core was found between the NGRIP (GICC05 chronologies) and previous cave $\delta^{18}O$ records (U-Th ages)[37]. The age difference reported here (150 ± 80 y) is comparable, but has much smaller uncertainty because of the substantial improvement in resolution and dating precision of the cave records used in this study. From the dynamic point of view, the synchroneity on a sub-centennial timescale between the initial onset/termination of HS4 in Greenland and CS4/SAS4 in mid-low latitude records hints towards a fast (decadal-scale) teleconnection via global atmospheric circulations (e.g., changes in the tropical Hadley circulation, meridional shifts of the ITCZ and the mid-latitude westerly wind belts in both hemispheres)[21,23,30,31,55,56]. In contrast, the longer (~500 y) and more gradual AM-AW onset (from ~40.2 to 39.4 ky BP) and termination (from ~38.3 to 38.0 ky BP) processes imply a slower (centennial-scale) oceanic reorganization in response to the abrupt North Atlantic climate change (e.g., changes in AMOC, subsequent South Ocean temperature and feedbacks)[20–23,29,57,58] (Figs. 2 and 3).

Records from the South American Monsoon domain. Over the tropical South Atlantic and in the SAM domain, SAS4, emerges as the most remarkable millennial-scale event, recording the highest amplitude of SST and monsoon precipitation variability during the last glacial[41,59]. Speleothem $\delta^{18}O$ records from the SAM domain spanning SAS4 are characterized by gradual shifts (Fig. 3 and Supplementary Fig. 6). Comparably, the SAS4 onset was initiated at ~40.19 ky BP, synchronous within uncertainty with CS4 (Fig. 1 and Supplementary Fig. 4). The SAS4 termination excursion in the SAM domain manifests as a progressive weakening of the SAM or decreasing rainfall[12,14,41] and a northward shift of the ITCZ[42,43]. Notably, the initial termination started apparently earlier than that of HS4/CS4 by ~250 y in Paraiso, Lapa Sem Fim, and El Condor records (Fig. 3 and Supplementary Figs. 5 and 6). Consistently, the growth interval of speleothems from Toca da Boa Vista/Toca da Barriguda cave (~40.1–38.6 ky BP) in Northeast Brazil provides precise constraints on the timing of a pluvial period, associated with a southward shift of the ITCZ[42,43] (Fig. 3 and Supplementary Fig. 6). The SAS4 structure in Northeast Brazil is characterized by an abrupt change (within 30 y) to a pluvial phase at ~39.5 ky BP[41,42], followed by a persistent increase in $\delta^{18}O$ (reflecting drier conditions), and eventually reaching the value of the early stage of SAS4 (or the growth phase I between 40.1 and 39.6 ky BP)[42] at ~38.6 ky BP. Intriguingly, growths of all stalagmites (e.g., TBV5, 14, 40 and 63 and TBR10-13)[42] ceased (Fig. 3 and Supplementary Fig. 6) prior to ~38.6 ky BP (corresponding to the start of abrupt $\delta^{18}O$ increase in the LSF13 record), suggesting that the hydroclimate became drier than during growth phase I[42], with an arid state comparable to pre-SAS4 and post-SAS4. The SAS4 pluvial phase, therefore, started approximately at the same time as counterparts in Greenland and AM-AW domains but terminated notably earlier. Additionally, Northeast Brazil is a semi-arid area whose precipitation variability is very sensitive to tropical South Atlantic sea-surface temperature (SST), and the earlier rainfall termination thus implies an earlier cooling in the tropical Western Equatorial Atlantic[59]. Collectively, the above observations are critical because the aforementioned sites are located in areas sensitive for tracking rainfall in South America including the Amazon Basin and thus Amazon River runoff into the Atlantic Ocean, as well as the ITCZ and tropical southwestern Atlantic SST (Fig. 4 and Supplementary Fig. 1).

Phasing between Antarctica and Greenland. Previous comparisons between Antarctic and Greenland ice-core records demonstrate that abrupt Greenland warming (cooling) led the corresponding onset of Antarctic cooling (warming) by ~200 ± 100 y (2σ)[21,29] or 122 ± 24 y (2σ)[59] in average for DO events, including HS and associated Antarctic hydroclimate variations. In a previous study, we have confirmed the coincidence between NGRIP ice-core $\delta^{18}O$, AM-AW speleothem $\delta^{18}O$, and atmospheric CH_4 across HS0/CS0 to within ± 20–40 y[23]. Using the same correlation strategy, we identified two corresponding breakpoints (see "Methods" section) in the CH_4 record from the West Antarctic Ice Sheet Divide ice-core (WDC) on the WD2014 chronology (Fig. 3 and Supplementary Fig. 7), and then matched them to the two anchor points at 40.20 ± 0.08 and 38.34 ± 0.07 ky BP by shifting the WD2014 chronology by 60 y to the younger side (Fig. 3). The high WDC accumulation rate provides high-resolution gas CH_4 and ice $\delta^{18}O$ data with small uncertainty on their age difference around HS4 period (±75 y)[60]. As such, the WDC ice $\delta^{18}O$ chronology around HS4 is precise and accurate at the sub-centennial-scale, provided that the CH_4 correlation to AM-AW and the Greenland records is robust, as tested on the decadal-scale by the previous HS0/CS0 study[23].

Two breakpoints are identified in the HS4 interval of the WDC $\delta^{18}O$ record (see "Methods" section) at ~39.87 and ~38.66 ky BP (Fig. 3 and Supplementary Fig. 7 and Supplementary Tables 1–3 and Supplementary Data 1). The breakpoint at 39.87 ky BP marks the warming onset associated with the HS4 onset in Antarctica consistent with other Antarctic records (Supplementary Fig. 7), which lags the HS4/CS4 initial onset (at 40.20 ± 0.08 ky BP) and associated atmospheric CH_4 change by ~300 y. This temporal relationship is similar to the interpolar phasing revealed previously for DO events, including HSs[21,29]. In contrast, the phasing relation surrounding the HS4 termination appears to be rather intricate. The breakpoint at ~38.66 ky BP (highest $\delta^{18}O$

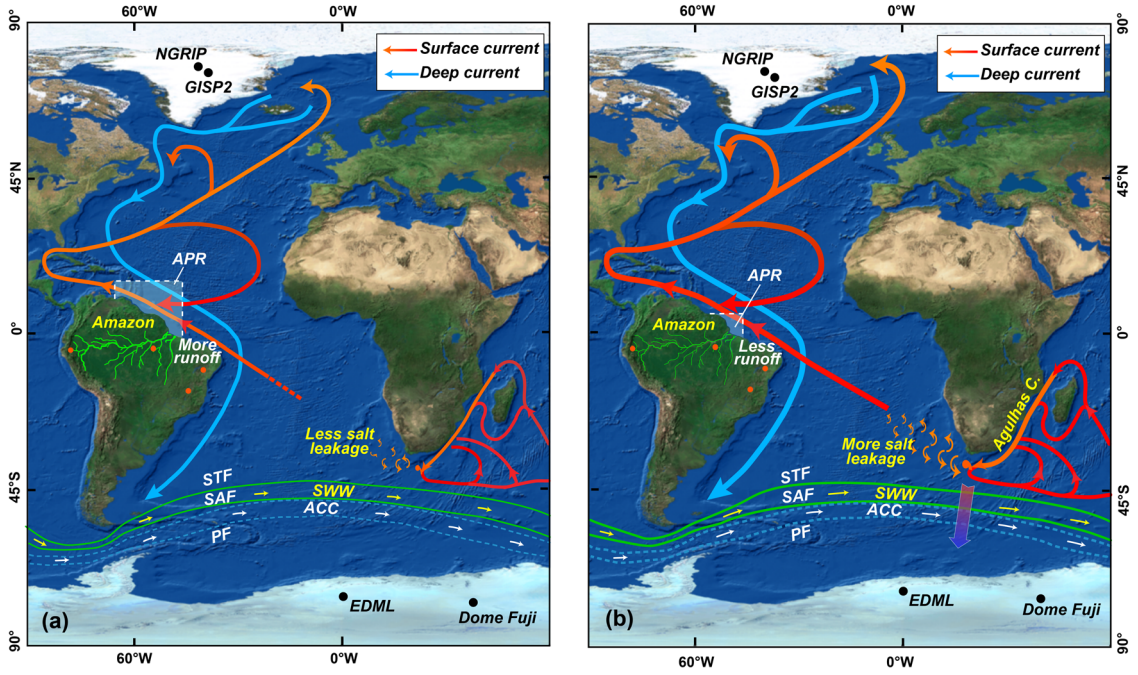

Fig. 4 Conceptual diagram depicting climatic dynamics surrounding the termination of HS4. a, **b** show centennial-scale changes in the Amazon River runoff and the SWW position prior to the abrupt HS4 termination in Greenland. The SWW and STF shifted poleward, which enhanced the Agulhas Current off the southern coast of South Africa, increased the Agulhas leakage and thus the salt/heat transport from the Indo-Pacific Ocean. Striking reduction of the Amazon runoff into the Atlantic Ocean, inferred from SAM records, increased the sea-surface salinity in the Amazon plume region (APR) and therefore increased the northward salt transport by the mean oceanic circulation (red route). Both processes ultimately contributed to AMOC strengthening. ACC Antarctic circumpolar current, SWW Southern Westerly wind, STF subtropical front, SAF Subantarctic front, PF Polar front. White dashed line in **a** depicts the modern APR, while the APR in **b** is rather arbitrary. Red dots show locations of SAM speleothem records of the South American Monsoon. Black dots show ice-core locations. The map was created using ArcGIS software and the world map background data are from the Environmental Systems Research Institute (ESRI, https://www.arcgis.com/apps/mapviewer/index.html?layers=10df2279f9684e4a9f6a7f08febac2a9).

value) or 38.64 ky BP (using the BREAKFIT algorithm)[49] in the WDC $\delta^{18}O$ record occurs ~300 y before the initial termination of HS4/CS4 at ~38.34 ± 0.07 ky BP (Fig. 3). This phasing relationship can be tested by the WDC CH_4 record on the same chronology (WD2014), due to a small uncertainty (±75 y) in the WDC ice-gas age difference[60] and a strong correlation of CH_4 with AM-AW and Greenland $\delta^{18}O$ records[23,44,60,61], controlled by the extent of wetlands and thus CH_4 emissions[62]. Essentially, the CH_4 initial jump associated with the HS4/CS4 termination lags the cooling onset (or hydroclimate changeover) inferred by $\delta^{18}O$ in the same ice-core by about 300 ± 75 y, suggesting an earlier change in the West Antarctic $\delta^{18}O$ record than the GS4/CS4 termination (Fig. 3 and Supplementary Figs. 3, 5, and 7 and Supplementary Tables 1–3 and Supplementary Data 1).

Notably, a spatial disparity emerges from the existing ice-core records from Antarctica. While the EDML, WDC, and DF records in Northwest Antarctica (related centrally to the Atlantic sector, especially EDML)[21] show a changeover (or cooling onset) hundreds of years earlier than the initial HS4/CS4 termination, TAL, and EDC records (related to the Pacific and the Indian Ocean sectors)[21] show a changeover a few hundred years after the initial HS4/CS4 termination (Supplementary Fig. 7). The spatially heterogeneous pattern is also shown in the 5-core average anomaly with two breakpoints, hundreds of years before and after the initial HS4/CS4 termination[21], similar to the Antarctic temperature stack (ATS) record that has two breakpoints as well[63] (Supplementary Fig. 7). The breakpoint after the HS4/CS4 termination is consistent with the previous notion that the abrupt Greenland warmings led the corresponding onset of Antarctic coolings by ~200 ± 100 y; however, the breakpoint before the Greenland termination, linked closely to the South Atlantic Ocean, occurred without any clear Greenland precursors (Supplementary Fig. 7). The underlying dynamics of the Antarctic heterogeneous pattern surrounding the HS4/CS4 termination remain unclear, possibly because of the special SWW pattern in the Atlantic sector[21], or regional effects, such as wind-driven changes to sea ice, gyre circulation or Weddell Sea deep convection[64]. Additional modeling and empirical studies are critically needed to further explore the mechanism(s).

Climate dynamics. In the chronological framework established here for HS4/CS4/SAS4, the associated onset of the Antarctic warming was ~300 y after the initial onset of HS4/CS4/SAS4 at ~40.20 ± 0.08 ky BP, suggesting a similar interpolar average phasing as observed previously for the DO events of the last glacial period[21,29]. Moreover, our analysis also provides evidence that mid-latitude to low-latitude hydroclimatic changes occurred synchronously within decades with abrupt changes in the North Atlantic, suggesting a fast teleconnection via meridional migrations of the Hadley circulation, ITCZ, and Westerlies in both hemispheres[20,21,23,30,55,56]. Conversely, the fact that AM-AW, SAM, and tropical hydroclimates show considerably longer and more gradual changes compared with Greenland also highlights a southward teleconnection influence from the northern high latitudes to the mid-low latitudes, which is in line with the role of the AMOC and the subsequent impacts on the monsoon systems[23,56,57,65,66], demonstrating one of the important aspects of the global thermal seesaw[20–23,29].

The events surrounding the HS4/CS4 termination are rather distinctive. On the basis of the correlation[23], the CS4 termination began at ~38.34 ky BP, synchronous with the abrupt northern

high-latitude temperature rise evident in Greenland ice-core records (Fig. 2). The more gradual change observed in the CS4 termination process suggests a southward propagation from northern high latitudes to mid-low latitudes, similar to the CS4 onset (Fig. 2). Furthermore, hydroclimate changes around the HS4/CS4 termination appear to be earlier in the SH, particularly in the SAM records as well as in Northwest Antarctic $\delta^{18}O$ records (Fig. 3 and Supplementary Figs. 6 and 7). This earlier changes in the SAM realm were likely linked to cooling in the Northwest Antarctica which is related closely to the Atlantic sector (Supplementary Fig. 7), shedding light on the HS4 termination dynamics. The Amazon River, originating mainly from the Amazon Basin and fed by SAM rainfall, is by far the largest river by volume of water (~6600 km^3 y^{-1}) in the world, representing ~17% of the global riverine discharge to the oceans. In the SAM domain, including the Amazon Basin, the SAS4 termination manifests as a persistent drying trend lasting ~250 y, which occurs mostly prior to the initial HS4/CS4 termination at ~38.34 ± 0.07 ky BP (Fig. 3 and Supplementary Fig. 5), consistent with marine records[67] (Supplementary Fig. 1). This observation suggests that the Amazon River discharge into the Atlantic Ocean decreased progressively for a few hundred years before the termination of HS4/CS4. Given the temporal relationship, the reduced discharge could plausibly act as a precursor of the HS4/SC4 termination. Lower freshwater input would increase the sea-surface salinity in the so-called Amazon Plume Region (APR)[68–70] and subsequently across the North Atlantic via increased northward salt transport by a shallow AMOC[71] or an overturning circulation involving the North Atlantic Intermediate Water (NAIW) in the late HS[72–75] (Fig. 4). The increased AMOC could have induced positive feedbacks via enhanced poleward heat transport, creating a positive temperature anomaly in the North Atlantic Ocean with a spatial structure similar to the positive phase of the Atlantic multidecadal variability (AMV) mode[76]. The persistence of a positive AMV mode would favor the development of a "seesaw" pattern in the Atlantic SST across the thermal equator, resulting in warming in the north and cooling in the south, thus displacing the ITCZ northward, further weakening the SAM, and reducing Amazon discharge[76]. Taken together, the above processes could eventually contribute to the resumption of a deep/strong AMOC mode, or the HS4/CS4 termination.

In contrast to Antarctic ice-core $\delta^{18}O$ records that show disparities in their changeover timing to cooling around the end of the HS4/CS4, Antarctic ice-core d_{ln} (a logarithmic definition of deuterium-excess) records show a rather coherent decreasing trend of several hundred years towards the Greenland HS4 termination (Supplementary Fig. 7). This suggests a progressive southward (poleward) shift of the strengthened SWW[21,30], or a positive Southern Annular Mode[77,78] that tends to propel a poleward shift of the subtropical front (STF) and a contraction of the SWW, thus weakening the winds at mid-latitudes (40°S to 50°S)[77–79]. As a result, the SWW off the southern coast of South Africa would shift poleward, which enhances the Agulhas Current and its salt/heat leakage to the Atlantic Ocean from the Indo-Pacific Ocean (the Agulhas Leakage). This process would further contribute to a gradual strengthening of the AMOC[35,80–84] (Fig. 4).

Modeling studies show that a precursory gradual shift in the AMOC system[85] may ultimately have reached a tipping point[86], allowing for an abrupt resumption of the deep/strong AMOC mode[26,27] and leading to the HS termination in the North Atlantic realm. Recent modeling and empirical studies also suggest a gradual recovery of the AMOC during the final part of HS events[87,88]. It remains unclear, however, if and how these gradual changes in the North Atlantic realm are dynamically linked to SH changes observed here because the present paucity of records with sufficient resolution and dating precision/accuracy precludes a precise comparison. We argue that the aforementioned SH changes were one of the important factors that contributed to the gradual recovery of the AMOC, which warrants further testing by model simulations.

Conclusions

The temporal constraints of CS4/SAS4 datasets presented here are characterized mostly by sub-centennial age precision, which together with a correlation strategy based on breakpoints, provides an improved chronological and interpretive framework to explain the dynamics of global ocean-atmosphere teleconnections associated with the signal propagations during HS4. The initial onset of this stadial occurred at ~40.20 ± 0.08 ky BP in the North Atlantic, synchronous within sub-centennial uncertainty with CS4/SAS4, implying a fast atmospheric teleconnection. In contrast, the longer and more gradual CS4/SAS4 onset suggests an oceanic reorganization in response to abrupt North Atlantic changes. The initial Antarctic warming appears to lag the initial HS4/CS4/SAS4 onset by ~300 y. These observations manifest a southward climatic teleconnection via both atmospheric and oceanic processes, from the northern high latitudes to the mid-low latitudes and finally the southern high latitudes. The initial termination of HS4/CS4 occurred at ~38.34 ± 0.07 ky BP and the dynamic relationship between HS4 and CS4 termination appears similar to their onset. Hundreds of years prior to the HS4/CS4 termination at ~38.34 ± 0.07 ky BP, however, the Amazon River discharge decreased and the SWW and STF shifted poleward. These precursor events, through positive feedbacks, gradually strengthened the AMOC and eventually culminated in deep/strong AMOC resumption and the abrupt HS4 termination in Greenland. In this regard, the initial trigger might reside in SH, suggesting a northward propagation from SH to the North Atlantic–AM-AW regions.

Methods

Paleoclimate records. We reconstructed or considerably improved ten speleothem $\delta^{18}O$ records spanning HS4. The sample information and cave settings are as follows: MSL from Hulu Cave (32°30′N, 119°10′E)[38], MWS-2 from Mawmluh Cave (25°16′N, 91°43′E)[39], ZJD171 from Zhangjia Cave (32°35′N, 105°58′E) and Wulu-30 from Wulu Cave (26°03′N, 105°05′E)[40] in the AM domain, and ELC-B from EL Condor Cave (5°56′S, 77°18′W)[12], PAR27 and PAR 15 from Paraiso Cave (4°04′S, 55°27′W)[14], LSF13 from Lapa Sem Fim Cave (16°09′S, 44°36′W)[41] and TBV5 and TBR10-13 from Toca da Boa Vista/Toca da Barriguda Caves (10°10′S, 40°52′W)[42,43] in the SAM domain (including the Amazon Basin) (Supplementary Fig. 1). Zhangjia cave is located near Guangyuan city, central-western China. The cave formed in limestones of the lower Triassic Feixianguan Formation. The columnar-shaped calcite stalagmite ZJD171, 22 cm in height and 6 cm in width, was collected in the first cave chamber, at ~800 m behind the cave entrance. According to instrumental records from Guangyuan meteorological station (~54 km southwest of the cave), the mean annual air temperature is 16.1 °C and the mean annual precipitation is ~950 mm, ~75% of which occurs during summer (June–September) (1951–2019). Cave monitoring results from 2017 to 2020 show a stable cave temperature of ~16.2 °C and constant relative humidity of ~100%.

U–Th dating method. Stalagmites were halved along the growth axis and polished. About 20–150 mg of powder was drilled near the central axis for each U–Th subsample. These subsamples were obtained by drilling the polished stalagmite section along the growth axis with a carbide dental burr. U–Th dating work was performed at the Isotope Laboratory, Xi'an Jiaotong University using multi-collector inductively coupled plasma mass spectrometers (MC-ICP-MS) (Thermo-Finnigan Neptune-*plus*). We used standard chemistry procedures to separate U and Th for dating[4]. A triple-spike (^{229}Th–^{233}U–^{236}U) isotope dilution method was employed to correct for instrumental fractionation and determine U–Th isotopic ratios and concentrations. The instrumentation, standardization and half-lives are reported in Cheng et al.[47,89]. All U–Th isotopes were measured on a MasCom multiplier behind the retarding potential quadrupole in peak-jumping mode. We followed similar procedures of characterizing the multiplier as described in Cheng et al.[47]. Uncertainties in U–Th isotopic data were calculated offline at the 2σ level, including corrections for blanks, multiplier dark noise, abundance sensitivity, and contents of the same nuclides in the spike solution. Corrected U–Th ages assume an initial $^{230}Th/^{232}Th$ atomic ratio of 4.4 ± 2.2 × 10^{-6}, the values for a

material at secular equilibrium with the bulk earth $^{232}Th/^{238}U$ value of 3.8. Most samples have high U/Th ratios and thus the corrections are negligible. A total of ~130 U–Th dates were obtained from eight speleothem samples (Supplementary Data 1). All dates are in stratigraphic order within error (Supplementary Fig. 2).

Age models. We used StalAge software[48] to construct age models for MWS-2, ZJD171, Wulu-30, ELC-B, PAR27, PAR15, and LSF13 records reported in this study (Supplementary Fig. 2). StalAge is particularly suited for speleothems creating objective age models based on two assumptions: (1) the age model is monotonic, and a straight line is fitted through all data or through as many data points as possible within error bars[48]. StalAge produces 300 realizations of age models by the Monte-Carlo simulation to account for the 95% confidence limits[48]. The major outliers are identified by disagreement with at least two data points and minor outliers are screened if more than 80% of the simulated straight lines fail to have a positive slope. In our case, no major or minor outliers were detected because all the ages in each age models increases monotonically within dating uncertainty. ZJD171 and PAR27 records contain hiatus between 39.24–39.95 and 38.84–39.56 ky BP, respectively. The StalAge were conducted separately for the ZJD171 (136.5–200.4 mm and 200.8–213.4 mm) and PAR27 sample (220.0–512.2 mm and 515.0–660.0 mm) records. The uncertainty is large (>200 y) in the boundary of sample MWS-2, ELC-B due to limited dating controls. Nonetheless, the key breakpoints (the initial HS4/CS4/SAS4 onset and termination) in detection periods are robust, which is away from the boundary areas and well constrained by several U–Th dates (Supplementary Fig. 2). The age model of MSL was constructed by Oxcal[90], consistent with previous publication[37]. Age models of TBV5 and TBR10-13 were constructed by linear interpolation.

Oxygen isotope analysis. For each oxygen isotope measurement, ~200 μg of powder was drilled from the sample. A total of ~3550 oxygen isotope ($\delta^{18}O$) subsamples were analyzed: ~600 from MWS-2, ~1020 from ZJD171, 243 from MSL, ~659 from PAR27, ~305 from PAR 15, 176 from LSF13, 297 from ELC-B, ~170 from TBV5 and ~110 from TBR10-13 (at Xi'an Jiaotong University); and ~263 from LSF13 (at the Instituto de Geociências, Universidade de São Paulo, Brazil) (Supplementary Data 1). Analyses carried out at Xi'an Jiaotong University used a Thermo-Finnigan MAT-253 mass spectrometer fitted with a Kiel Carbonate Device IV. In Universidade de São Paulo, sample oxygen isotopes were analyzed with an online, automated, carbonate preparation system linked to a Finnigan Delta Plus Advantage mass spectrometer. The $\delta^{18}O$ values are reported in per mil (‰) deviations, relative to the Vienna Pee Dee Belemnite (VPDB) standard. All subsamples were calibrated against standards, and the long-term reproducibility for $\delta^{18}O$ measurements over the course of this study (~1 y) was typically ~0.1‰ (1σ).

Breakpoint determination. We used three methods to identify the timings and age uncertainty of initial onset and termination of CS4/SAS4 from the AM-AW and SAM domains. Method 1: Through visual inspection, we picked the minima (maxima) in different records between 40.0 and 40.4 ky BP indicating the beginning of persistent positive (negative) excursions in the AM-AW (SAM) records marking the initial onset of CS4/SAS4. Similarly, we chose the maxima (minima) in the records between 39.0 to 38.2 ky BP indicating the beginning of persistent negative (positive) excursions in the AM-AW (SAM) records marking the initial termination of CS4/SAS4. The age uncertainties of these points were calculated by combing 2σ uncertainty and error-weighted mean uncertainty quadratically, which reflect the age model uncertainty and partially the proxy time-series "noise". Method 2: We used BREAKFIT[49] algorithm to identify the onset and termination of HS4/CS4/SAS4 in various speleothem and ice-core records. The algorithm employs a continuous function, consisting of two linear parts that are joined at the breakpoint. The break model is fitted to data using a weighted least-squares method with a brute-force search for the breakpoint. While BREAKFIT provides an objective estimate for the change points in a given dataset, the choice of "fit interval" is subjective and can influence the results. The main criteria to choose analytical time intervals are as follows: (1) the interval contains one breakpoint, and (2) use the same time intervals for records from the same region if possible. Though BREAKFIT algorithm can give statistical uncertainties in the timing of breakpoints using 2000 block bootstrap simulations, which preserved the distribution and serial dependence of the data over the length of a block (Supplementary Tables 1 and 2), it does not take into account the dating uncertainty associated with the record. Additionaly, the differences in $\delta^{18}O$ records from each domain, referred here as the "noise", also contribute to the uncertainty. To account for these additional sources of uncertainties, we conducted the BREAKFIT analysis for our speleothem records using the mean (50th) as well as the 2.5th and 97.5th percentile of age model ensemble of each record. The final breakpoint and 2σ uncertainty of each record was determined by the mean and standard deviation of three BREAKFIT results. The uncertainty mainly encompasses the age model uncertainty. Method 3: To further assess both the dating uncertainty and the noise of records within each domain, we z-scored and composited the record from the same climate domain as follows. We combined the ZJD171, MWS-2, and Wulu30 records as the representative of the AM-AW domain, and the PAR15, PAR27, LSF13, and ELC-B records as the representative of the SAM domain. For each domain, we again conducted the BREAKFIT analysis on the composite record using the 2.5th, 5th, and 97.5th percentile of age model ensemble. The final breakpoint and σ uncertainty were determined by the mean and standard deviation of the three BREAKFIT results. The reported uncertainties incorporate uncertainties from the age model and proxy time-series noise. The selected time intervals for BREAKFIT analyses are listed in Supplementary Tables 1–3. Results and additional discussion are presented in Supplementary Figs. 4 and 5 and Supplementary Tables 1–3. Generally, breakpoints determined via BREAKFIT algorithms agree well with visual inspections.

Correlation strategy. The direct comparison between AM-AW and North Atlantic records supports the correlation strategy via matching "breakpoints"[23,53] rather than their "mid-points"[13,29] (Supplementary Fig. 3).

Data availability

The new data used in this study are reported in Supplementary Data 1, and will be available at https://www.ncdc.noaa.gov/paleo/study/34255

Code availability

A version of the breakfit software (without timescale simulation)[49] is freely available via the Climate Risk Analysis website (https://www.mudelsee.com). The algorithm of age-model (StalAge)[48] is written in the open source statistical software R (https://cloud.r-project.org).

Received: 29 May 2021; Accepted: 19 October 2021;
Published online: 08 November 2021

References

1. Rasmussen, S. O. et al. A stratigraphic framework for abrupt climatic changes during the Last Glacial period based on three synchronized Greenland ice-core records: refining and extending the INTIMATE event stratigraphy. *Quat. Sci. Rev.* **106**, 14–28 (2014).
2. Hemming, S. R. Heinrich events: massive late Pleistocene detritus layers of the North Atlantic and their global climate imprint. *Rev. Geophys.* https://doi.org/10.1029/2003RG000128 (2004).
3. Heinrich, H. Origin and consequences of cyclic ice rafting in the northeast Atlantic Ocean during the past 130,000 years. *Quat. Res.* **29**, 142–152 (1988).
4. Edwards, R. L., Chen, J., Ku, T.-L. & Wasserburg, G. Precise timing of the last interglacial period from mass spectrometric determination of thorium-230 in corals. *Science* **236**, 1547–1553 (1987).
5. Hodell, D. A. et al. Anatomy of Heinrich Layer 1 and its role in the last deglaciation. *Paleoceanography* **32**, 284–303 (2017).
6. Barker, S. et al. Interhemispheric Atlantic seesaw response during the last deglaciation. *Nature* **457**, 1097–1102 (2009).
7. Asmerom, Y., Polyak, V. J. & Burns, S. J. Variable winter moisture in the southwestern United States linked to rapid glacial climate shifts. *Nat. Geosci.* **3**, 114–117 (2010).
8. Genty, D. et al. Precise dating of Dansgaard–Oeschger climate oscillations in western Europe from stalagmite data. *Nature* **421**, 833–837 (2003).
9. Allen, J. R. et al. Rapid environmental changes in southern Europe during the last glacial period. *Nature* **400**, 740–743 (1999).
10. Benson, L. V. et al. Climatic and hydrologic oscillations in the Owens Lake Basin and adjacent Sierra Nevada, California. *Science* **274**, 746–749 (1996).
11. Cheng, H. et al. A penultimate glacial monsoon record from Hulu Cave and two-phase glacial terminations. *Geology* **34**, 217 (2006).
12. Cheng, H. et al. Climate change patterns in Amazonia and biodiversity. *Nat. Commun.* **4**, 1411 (2013).
13. Wang, Y. J. et al. A high-resolution absolute-dated late Pleistocene Monsoon record from Hulu Cave, China. *Science* **294**, 2345–2348 (2001).
14. Wang, X. et al. Hydroclimate changes across the Amazon lowlands over the past 45,000 years. *Nature* **541**, 204–207 (2017).
15. Deplazes, G. et al. Links between tropical rainfall and North Atlantic climate during the last glacial period. *Nat. Geosci.* **6**, 213–217 (2013).
16. Kanner, L. C., Burns, S. J., Cheng, H. & Edwards, R. L. High-latitude forcing of the South American summer monsoon during the last glacial. *Science* **335**, 570–573 (2012).
17. Leduc, G. et al. Moisture transport across Central America as a positive feedback on abrupt climatic changes. *Nature* **445**, 908–911 (2007).
18. Cruz, F. W. et al. Insolation-driven changes in atmospheric circulation over the past 116,000 years in subtropical Brazil. *Nature* **434**, 63–66 (2005).
19. Brook, E. J. & Buizert, C. Antarctic and global climate history viewed from ice cores. *Nature* **558**, 200–208 (2018).
20. Pedro, J. B. et al. Beyond the bipolar seesaw: toward a process understanding of interhemispheric coupling. *Quat. Sci. Rev.* **192**, 27–46 (2018).

21. Buizert, C. et al. Abrupt ice-age shifts in southern westerly winds and Antarctic climate forced from the north. *Nature* **563**, 681–685 (2018).
22. Stocker, T. F. & Johnsen, S. J. A minimum thermodynamic model for the bipolar seesaw. *Paleoceanography* **18**, 4 (2003).
23. Cheng, H. et al. Timing and structure of the Younger Dryas event and its underlying climate dynamics. *Proc. Natl Acad. Sci. USA* **117**, 23408–23417 (2020).
24. MacAyeal, D. Binge/purge oscillations of the Laurentide ice sheet as a cause of the North Atlantic's Heinrich events. *Paleoceanography* **8**, 775–784 (1993).
25. Stoner, J. S., Channell, J. E. & Hillaire-Marcel, C. The magnetic signature of rapidly deposited detrital layers from the deep Labrador Sea: relationship to North Atlantic Heinrich layers. *Paleoceanography* **11**, 309–325 (1996).
26. Henry, L. et al. North Atlantic ocean circulation and abrupt climate change during the last glaciation. *Science* **353**, 470–474 (2016).
27. McManus, J. F., Francois, R., Gherardi, J.-M., Keigwin, L. D. & Brown-Leger, S. Collapse and rapid resumption of Atlantic meridional circulation linked to deglacial climate changes. *Nature* **428**, 834–837 (2004).
28. Broecker, W. S., Peteet, D. M. & Rind, D. Does the ocean–atmosphere system have more than one stable mode of operation? *Nature* **315**, 21–26 (1985).
29. Members, W. D. P. Precise interpolar phasing of abrupt climate change during the last ice age. *Nature* **520**, 661–665 (2015).
30. Markle, B. R. et al. Global atmospheric teleconnections during Dansgaard–Oeschger events. *Nat. Geosci.* **10**, 36–40 (2017).
31. Capron, E. et al. The anatomy of past abrupt warmings recorded in Greenland ice. *Nat. Commun.* **12**, 2106 (2021).
32. Zhang, X., Knorr, G., Lohmann, G. & Barker, S. Abrupt North Atlantic circulation changes in response to gradual CO_2 forcing in a glacial climate state. *Nat. Geosci.* **10**, 518–523 (2017).
33. Peltier, W. R. & Vettoretti, G. Dansgaard-Oeschger oscillations predicted in a comprehensive model of glacial climate: a "kicked" salt oscillator in the Atlantic. *Geophys. Res. Lett.* **41**, 7306–7313 (2014).
34. Vellinga, M. & Wu, P. Low-latitude freshwater influence on centennial variability of the Atlantic thermohaline circulation. *J. Clim.* **17**, 4498–4511 (2004).
35. Knorr, G. & Lohmann, G. Southern Ocean origin for the resumption of Atlantic thermohaline circulation during deglaciation. *Nature* **424**, 532–536 (2003).
36. Schmidt, M. W., Spero, H. J. & Lea, D. W. Links between salinity variation in the Caribbean and North Atlantic thermohaline circulation. *Nature* **428**, 160–163 (2004).
37. Adolphi, F. et al. Connecting the Greenland ice-core and U/Th timescales via cosmogenic radionuclides: testing the synchroneity of Dansgaard–Oeschger events. *Clim. Past* **14**, 1755–1781 (2018).
38. Cheng, H. et al. Atmospheric $^{14}C/^{12}C$ changes during the last glacial period from Hulu Cave. *Science* **362**, 1293–1297 (2018).
39. Jaglan, S. et al. Abrupt Indian summer monsoon shifts aligned with Heinrich events and D-O cycles since MIS 3. *Palaeogeogr. Palaeoclimatol. Palaeoecol.* **583**, 110658 (2021).
40. Liu, D. et al. Contrasting patterns in abrupt Asian summer monsoon changes in the last glacial period and the Holocene. *Paleoceanogr. Paleoclimatol.* **33**, 214–226 (2018).
41. Stríkis, N. M. et al. South American monsoon response to iceberg discharge in the North Atlantic. *Proc. Natl Acad. Sci.* **115**, 3788–3793 (2018).
42. Wendt, K. A. et al. Three-phased Heinrich Stadial 4 recorded in NE Brazil stalagmites. *Earth Planet. Sci. Lett.* **510**, 94–102 (2019).
43. Wang, X. et al. Wet periods in northeastern Brazil over the past 210 kyr linked to distant climate anomalies. *Nature* **432**, 740–743 (2004).
44. Cheng, H. et al. The Asian monsoon over the past 640,000 years and ice age terminations. *Nature* **534**, 640–646 (2016).
45. Cheng, H., Sinha, A., Wang, X., Cruz, F. W. & Edwards, R. L. The Global Paleomonsoon as seen through speleothem records from Asia and the Americas. *Clim. Dyn.* **39**, 1045–1062 (2012).
46. Cheng, H. et al. Chinese stalagmite paleoclimate researches: a review and perspective. *Sci. China Earth Sci.* **62**, 1489–1513 (2019).
47. Cheng, H. et al. Improvements in ^{230}Th dating, ^{230}Th and ^{234}U half-life values, and U–Th isotopic measurements by multi-collector inductively coupled plasma mass spectrometry. *Earth Planet. Sci. Lett.* **371–372**, 82–91 (2013).
48. Scholz, D. & Hoffmann, D. L. StalAge–An algorithm designed for construction of speleothem age models. *Quat. Geochronol.* **6**, 369–382 (2011).
49. Mudelsee, M. Break function regression. *Eur. Phys. J. Spec. Top.* **174**, 49–63 (2009).
50. Fleitmann, D. et al. Timing and climatic imprint of Dansgaard-Oeschger events in stalagmites from Northern Turkey. *Geophys. Res. Lett.* **36**, L19707 (2009).
51. Rasmussen, S. O. et al. A new Greenland ice core chronology for the last glacial termination. *J. Geophys. Res.* https://doi.org/10.1029/2005JD006079 (2006).
52. Abbott, P. M. & Davies, S. M. Volcanism and the Greenland ice-cores: the tephra record. *Earth Sci. Rev.* **115**, 173–191 (2012).
53. Du, W. et al. Timing and structure of the weak Asian Monsoon event about 73,000 years ago. *Quat. Geochronol.* **53**, 101003 (2019).
54. Svensson, A. et al. The Greenland ice core chronology 2005, 15–42 ka. Part 2: comparison to other records. *Quat. Sci. Rev.* **25**, 3258–3267 (2006).
55. Ceppi, P., Hwang, Y. T., Liu, X., Frierson, D. M. & Hartmann, D. L. The relationship between the ITCZ and the Southern Hemispheric eddy-driven jet. *J. Geophys. Res.* **118**, 5136–5146 (2013).
56. Chiang, J. C., Lee, S.-Y., Putnam, A. E. & Wang, X. South Pacific Split Jet, ITCZ shifts, and atmospheric North–South linkages during abrupt climate changes of the last glacial period. *Earth Planet. Sci. Lett.* **406**, 233–246 (2014).
57. Broccoli, A. J., Dahl, K. A. & Stouffer, R. J. Response of the ITCZ to Northern Hemisphere cooling. *Geophys. Res. Lett.* https://doi.org/10.1029/2005GL024546 (2006).
58. Chiang, J. C. & Bitz, C. M. Influence of high latitude ice cover on the marine intertropical convergence zone. *Clim. Dyn.* **25**, 477–496 (2005).
59. Venancio, I. M. et al. Ocean-atmosphere interactions over the western South Atlantic during Heinrich stadials. *Glob. Planet. Change* **195**, 103352 (2020).
60. Buizert, C. et al. The WAIS Divide deep ice core WD2014 chronology–Part 1: methane synchronization (68–31 ka BP) and the gas age–ice age difference. *Clim. Past* **11**, 153–173 (2015).
61. Cheng, H. et al. Ice age terminations. *Science* **326**, 248–252 (2009).
62. Petrenko, V. V. et al. Minimal geological methane emissions during the Younger Dryas–Preboreal abrupt warming event. *Nature* **548**, 443–446 (2017).
63. Parrenin, F. et al. Synchronous change of atmospheric CO_2 and Antarctic temperature during the last deglacial warming. *Science* **339**, 1060–1063 (2013).
64. Lefebvre, W., Goosse, H., Timmermann, R. & Fichefet, T. Influence of the Southern Annular Mode on the sea ice–ocean system. *J. Geophys. Res.* https://doi.org/10.1029/2004JC002403 (2004).
65. Cai, Y. et al. High-resolution absolute-dated Indian Monsoon record between 53 and 36 ka from Xiaobailong Cave, southwestern China. *Geology* **34**, 621–624 (2006).
66. Rohling, E. J. et al. Controls on the East Asian monsoon during the last glacial cycle, based on comparison between Hulu Cave and polar ice-core records. *Quat. Sci. Rev.* **28**, 3291–3302 (2009).
67. Zhang, Y. et al. Different precipitation patterns across tropical South America during Heinrich and Dansgaard-Oeschger stadials. *Quat. Sci. Rev.* **177**, 1–9 (2017).
68. Giffard, P., Llovel, W., Jouanno, J., Morvan, G. & Decharme, B. Contribution of the Amazon river discharge to regional sea level in the tropical Atlantic Ocean. *Water* **11**, 2348 (2019).
69. Liang, Y.-C. et al. Amplified seasonal cycle in hydroclimate over the Amazon river basin and its plume region. *Nat. Commun.* **11**, 1–11 (2020).
70. Masson, S. & Delecluse, P. Influence of the Amazon river runoff on the tropical Atlantic. *Phys. Chem. Earth Part B* **26**, 137–142 (2001).
71. Broecker, W. S. Global change and oceanography programs. *Science* **254**, 1566–1566 (1991).
72. Burckel, P. et al. Changes in the geometry and strength of the Atlantic meridional overturning circulation during the last glacial (20–50 ka). *Climate Past* **12**, 2061–2075 (2016).
73. Skinner, L., Menviel, L., Broadfield, L., Gottschalk, J. & Greaves, M. Southern Ocean convection amplified past Antarctic warming and atmospheric CO_2 rise during Heinrich Stadial 4. *Commun. Earth Environ.* **1**, 1–8 (2020).
74. Turney, C. S. et al. Early Last Interglacial ocean warming drove substantial ice mass loss from Antarctica. *Proc. Natl Acad. Sci.* **117**, 3996–4006 (2020).
75. Waelbroeck, C. et al. Relative timing of precipitation and ocean circulation changes in the western equatorial Atlantic over the last 45 kyr. *Clim. Past* **14**, 1315–1330 (2018).
76. Jahfer, S., Vinayachandran, P. & Nanjundiah, R. S. The role of Amazon river runoff on the multidecadal variability of the Atlantic ITCZ. *Environ. Res. Lett.* **15**, 054013 (2020).
77. Davies, B. J. et al. The evolution of the Patagonian Ice Sheet from 35 ka to the present day (PATICE). *Earth Sci. Rev.* **204**, 103152 (2020).
78. Moreno, P. et al. Onset and evolution of southern annular mode-like changes at centennial timescale. *Sci. Rep.* **8**, 1–9 (2018).
79. Toggweiler, J. R. & Russell, J. Ocean circulation in a warming climate. *Nature* **451**, 286–288 (2008).
80. Bard, E. & Rickaby, R. E. Migration of the subtropical front as a modulator of glacial climate. *Nature* **460**, 380–383 (2009).
81. Biastoch, A., Böning, C. W., Schwarzkopf, F. U. & Lutjeharms, J. R. E. Increase in Agulhas leakage due to poleward shift of Southern Hemisphere westerlies. *Nature* **462**, 495–498 (2009).
82. Peeters, F. J. et al. Vigorous exchange between the Indian and Atlantic oceans at the end of the past five glacial periods. *Nature* **430**, 661–665 (2004).
83. Simon, M. H. et al. Millennial-scale Agulhas Current variability and its implications for salt-leakage through the Indian–Atlantic Ocean Gateway. *Earth Planet. Sci. Lett.* **383**, 101–112 (2013).

84. Weldeab, S., Schneider, R. R. & Kölling, M. Deglacial sea surface temperature and salinity increase in the western tropical Atlantic in synchrony with high latitude climate instabilities. *Earth Planet. Sci. Lett.* **241**, 699–706 (2006).
85. Muschitiello, F. et al. Deep-water circulation changes lead North Atlantic climate during deglaciation. *Nat. Commun.* **10**, 1–10 (2019).
86. Boulton, C. A., Allison, L. C. & Lenton, T. M. Early warning signals of Atlantic Meridional overturning circulation collapse in a fully coupled climate model. *Nat. Commun.* **5**, 1–9 (2014).
87. Margari, V. et al. Fast and slow components of interstadial warming in the North Atlantic during the last glacial. *Commun. Earth Environ.* **1**, 1–9 (2020).
88. Menviel, L., Timmermann, A., Friedrich, T. & England, M. Hindcasting the continuum of Dansgaard–Oeschger variability: mechanisms, patterns and timing. *Clim. Past* **10**, 63–77 (2014).
89. Cheng, H. et al. The half-lives of uranium-234 and thorium-230. *Chem. Geol.* **169**, 17–33 (2000).
90. Ramsey, C. B. Deposition models for chronological records. *Quat. Sci. Rev.* **27**, 42–60 (2008).
91. Bauska, T. K., Marcott, S. A. & Brook, E. J. Abrupt changes in the global carbon cycle during the last glacial period. *Nat. Geosci.* **14**, 91–96 (2021).
92. Markle, B. R., Steig, E. J., Roe, G. H., Winckler, G. & McConnell, J. R. Concomitant variability in high-latitude aerosols, water isotopes and the hydrologic cycle. *Nat. Geosci.* **11**, 853–859 (2018).

Acknowledgements

This work was supported by NSFC grants 41731174 and 41888101 to H.C. We sincerely thank Dr. Luke Skinner for his very constructive comments and suggestions. The tourism authorities provide the permissions and supports to field work and sampling collections.

Author contributions

H.C. obtained funding, conducted the field work, and conceptualized this study. Y.X., X.D., J.Z., H.L. W.D., B.Z., X.J. and C.S. carried the experiments and data analysis. J.Z., H.Z, G.K., N.M.S., F.W.C., A.S.A., X.W., S.D., D.L., R.K.S. and S.J. helped organize fieldwork, sampling and provide samples. J.B., A.S., Y.C., F.W.C., A.K.G, R.L.E. and Z.L. interpreted results, H.C. accomplished the writing with the help of all co-authors.

Competing interests

The authors declare no competing interests.

Additional information

Supplementary information The online version contains supplementary material available at https://doi.org/10.1038/s43247-021-00304-6.

Correspondence and requests for materials should be addressed to Hai Cheng.

Peer review information *Communications Earth & Environment* thanks Xiunlin Yang, Luke Skinner and the other, anonymous, reviewer(s) for their contribution to the peer review of this work. Primary Handling Editor: Joe Aslin.

Reprints and permission information is available at http://www.nature.com/reprints

Publisher's note Springer Nature remains neutral with regard to jurisdictional claims in published maps and institutional affiliations.